

Crystalline phase transition in as-synthesized pure silica zeolite RTH containing tetra-alkyl phosphonium as organic structure directing agent

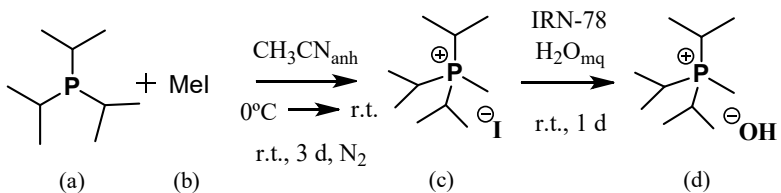
*Joaquin Martínez-Ortigosa¹, Reisel Millán¹, Jorge Simancas¹, Manuel Hernández-Rodríguez¹, J. Alejandro Vidal-Moya¹, Jose L. Jordá¹, Charlotte Martineau-Corcos^{2,3}
Vincent Sarou-Kanian³, Mercedes Boronat¹, Teresa Blasco¹, Fernando Rey¹*

¹Instituto de Tecnología Química, Universitat Politècnica de València - Consejo Superior de Investigaciones Científicas (UPV-CSIC), Avda. de los Naranjos s/n, 46022 Valencia, Spain.

²CortecNet, Les Ulis, 7 avenue du Hoggar, 91940 Les Ulis, France.

³CEMHTI-CNRS, CNRS UPR3079, 1D Avenue de la Recherche Scientifique, 45071 Orléans cedex 2, France.

Synthesis and characterization of the triisopropyl(methyl)phosphonium hydroxyde.



Schematic synthesis of the organic structure directing agent methyl-tri-isopropylphosphonium cation.

Theoretical and experimental chemical composition of the triisopropyl(methyl)phosphonium iodide.

| C ₁₀ H ₂₄ PI | % C (wt %) | % P (wt %) | % H (wt %) | C/P molar ratio |
|------------------------------------|------------|------------|------------|-----------------|
| Theoretical | 39.7 | 10.2 | 8.0 | 10 |
| Experimental | 40.1 | 9.1 | 8.5 | 11.3 |

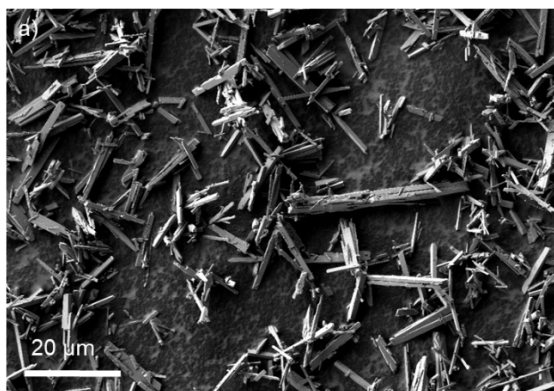
NMR characterization of the triisopropyl(methyl)phosphonium iodide

¹H NMR (D₂O): a: 1.26 ppm (dd, 18xH, P(CH(CH₃)₂)₃); b: 1.64 ppm (d, 3xH, PCH₃), c: 2.63 ppm (dv, 3xH, P(CH(CH₃)₂)₃).

¹³C NMR (D₂O): A: 0.34 ppm (d, P(CH(CH₃)₂)₃); B: 17.96 ppm (d, P(CH(CH₃)₂)₃); C: 22.40 ppm (d, PCH₃).

³¹P NMR (D₂O): 44.55 ppm (s, H decoupl.).

RTH-9



RTH-30

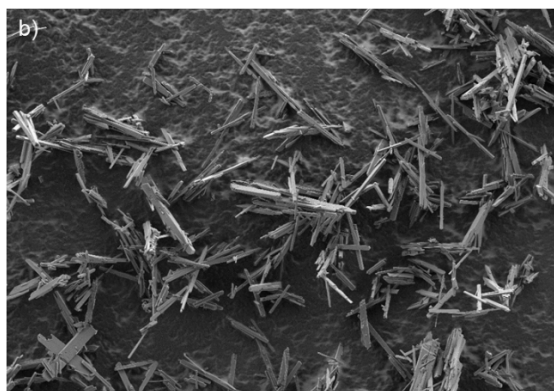


Figure S1. FESEM images of the RTH-9 (left) and RTH-30 (right) zeolites (both images have the same scale).

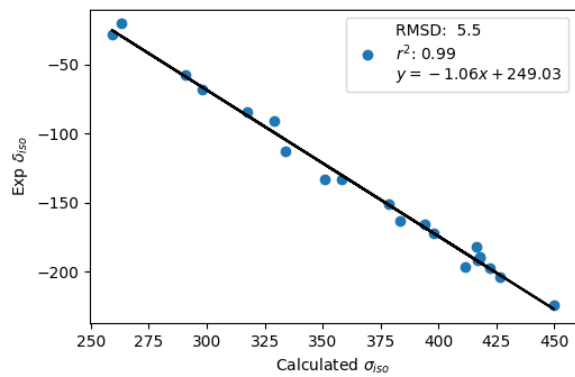


Figure S2. Correlation between experimental isotropic chemical shifts δ_{iso} and theoretically NMR shielding calculated with TB-mBJ exchange potential (σ_{iso}) (in ppm) for ^{19}F in fluorinated compounds. All structures are optimized with PBE-D3. The references for the experimental values of ^{19}F are indicated in **Table S1**.

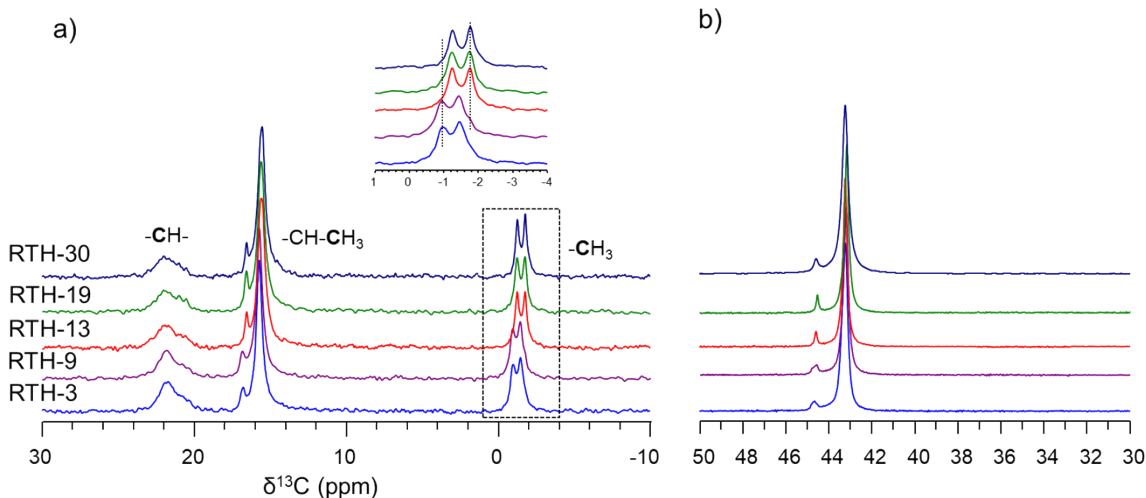
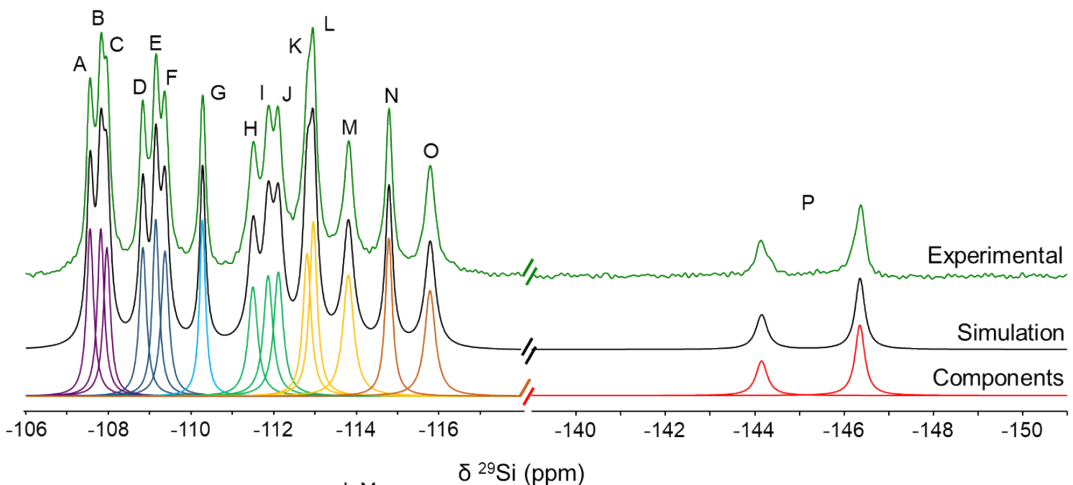


Figure S3. a) ^1H - ^{13}C CP MAS NMR spectra of the RTH samples and the assignment to the different groups of the P-OSDA $^+$ cation; the inset of the figure shows the amplification of signal of $-\text{CH}_3$ and b) ^{31}P MAS NMR spectra of the RTH samples.

The ^1H - ^{13}C cross polarization (CP) MAS NMR spectra, $v_0(^{13}\text{C}) = 100.6$ MHz and $v_0(^1\text{H}) = 400.1$ MHz, were carried out in a 4 mm probe spinning the samples at 10 kHz, using ^1H $\pi/2$ pulse length of 2.3 μs , 2 ms contact time, SPINAL to decouple ^1H nuclei and recycle delays of 3 s. The ^{31}P spectra, $v_0(^{31}\text{P}) = 161.9$ MHz, were recorded using a 4 mm probe spinning the samples at 10 kHz, using 20 s as recycle delay, ^{31}P $\pi/2$ pulse length of 4.0 μs and SPINAL for ^1H decoupling.

Figure S3a display the ^{13}C MAS NMR spectra of the RTH-x zeolites obtained at different synthesis time. The splitting of the $\equiv\text{P}-\text{CH}_3$ signal is due to the scalar J -coupling with the ^{31}P ($I = 1/2$) $J_{\text{C},\text{P}} = 49$ Hz. The $\delta^{13}\text{C}$ of the signal assigned to the isolated $-\text{CH}_3$ group of the P-OSDA $^+$ (inset of the **Figure S3a**) is slightly different for the RTH samples, suggesting a little variation in their orientation inside the cavities. The ^{31}P MAS NMR spectra of the RTH-x samples **Figure S3b** consist of a main signal at $\delta^{31}\text{P} = 43.2$ ppm and another one much weaker at $\delta^{31}\text{P} = 44.6$ ppm suggesting that some phosphorous are in a slightly different environment.

a)



b)

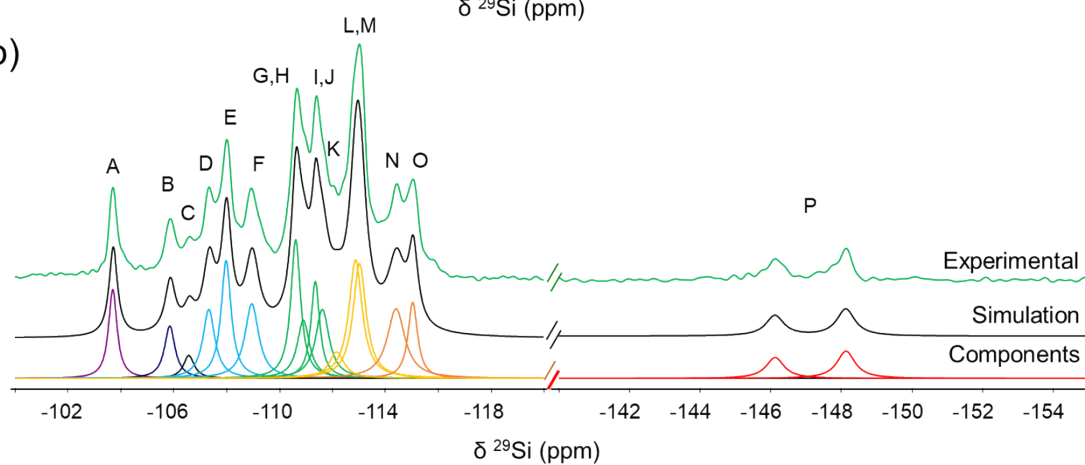


Figure S4. Simulation of the ^{29}Si MAS NMR spectra of the zeolites a) RTH-30 and b) RTH-9. A total of 16 Lorentzian signals of equal intensity, 15 of them in the Q⁴ region and one of penta-coordinated silicon have been used. Note that the scale in both spectra is different

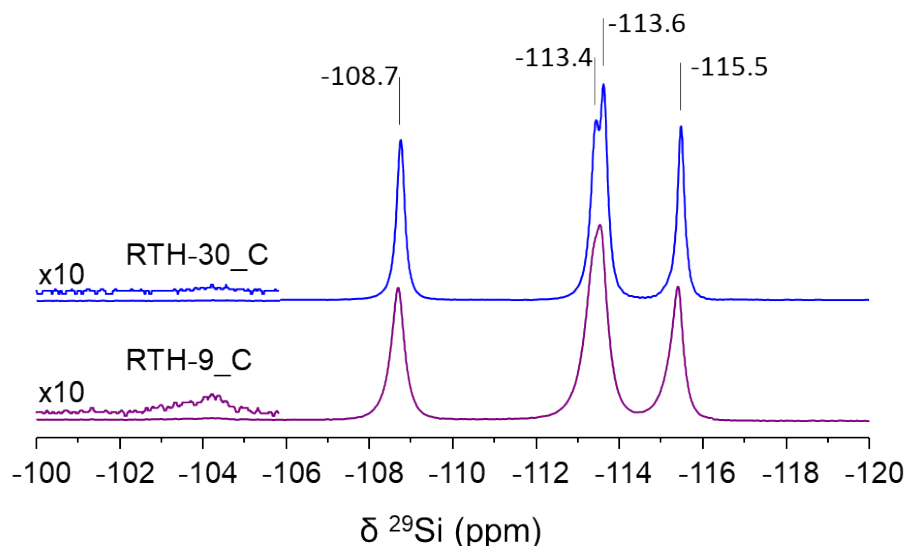


Figure S5. ^{29}Si MAS NMR spectra of the zeolites RTH-30 (top) and RTH-9 (down) thermally treated under hydrogen at 750 °C and subsequently calcined in air at 700 °C.

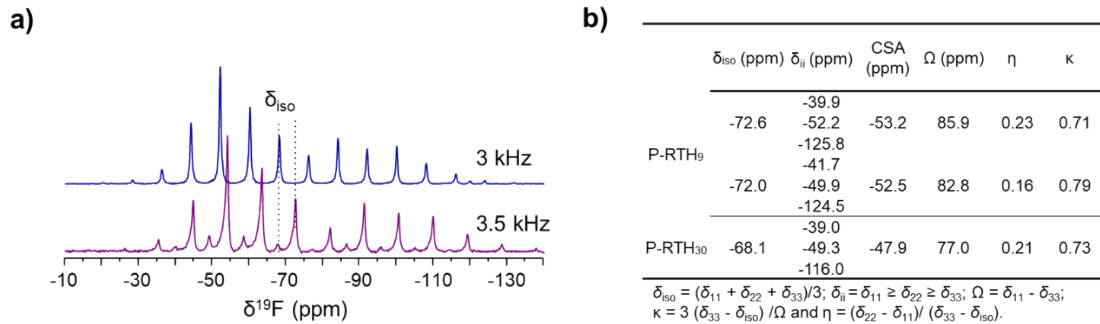


Figure S6. a) ^{19}F MAS NMR spectra of the zeolite RTH-30 (blue) and RTH-9 (purple) recorded at the spinning rates indicated in the figure. b) CSA parameters obtained from the simulation of the spectra shown in a).

Recording the ^{19}F NMR spectra at low spinning rates do not average out the chemical shift anisotropy (CSA) giving rise to spinning side bands (SSB) with a contour shape that reflects the local symmetry of the fluoride anions. **Figure S6a** compares the ^{19}F MAS-NMR spectra of the RTH-9 and RTH-30 zeolites, recorded at 3.5 and 3 kHz spinning rates, respectively. The spectrum of the RTH-30 zeolite was simulated by using a unique component with $\delta^{19}\text{F}_{\text{iso}} = -68.1$ ppm and that of the RTH-9 zeolite with two components at $\delta^{19}\text{F}_{\text{iso}} = -72.6$ ppm and $\delta^{19}\text{F}_{\text{iso}} = -72.0$ ppm ignoring the tiny contribution at $\delta^{19}\text{F}_{\text{iso}} = -67.2$ ppm. The CSA parameters obtained in the simulation of the spinning side bands (SSB) patterns are shown in **Figure S6b**. The $\eta \approx 0.2$ and $\kappa \approx 0.7$ values are characteristic of an axial symmetry¹⁻³ and the *span*, $\Omega = 77.0 - 86.0$ ppm, higher than 70.0 ppm is consistent with occurrence of Si-F bonding ($\text{O}_4\text{Si}-\text{F}$ species).⁴ The Ω values for a mobile F^- atoms in as-prepared zeolites ranges between 45 - 65 ppm as reported previously for MFI and CHA zeolites.

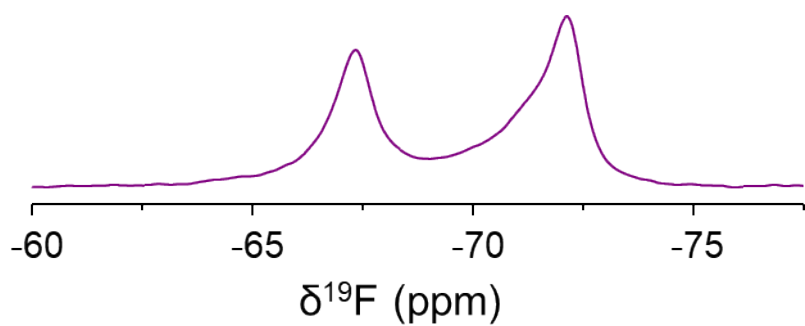


Figure S7. ^{19}F MAS NMR spectrum of the RTH zeolite synthesized with P-SODA $^+$ by heating the gel at 150 °C for 15 days (RTH(150)-15 sample).

The ^{19}F NMR spectrum of the RTH(150)-15 sample synthesized following the procedure depicted in the experimental part but heating at 150 °C (instead of 175 °C) during 15 days contains two signals at $\delta^{19}\text{F} = -67.3$ and $\delta^{19}\text{F} = -71.8$ ppm with practically equal intensity indicating the presence of similar amounts of *RTH-A* and *RTH-B* phases

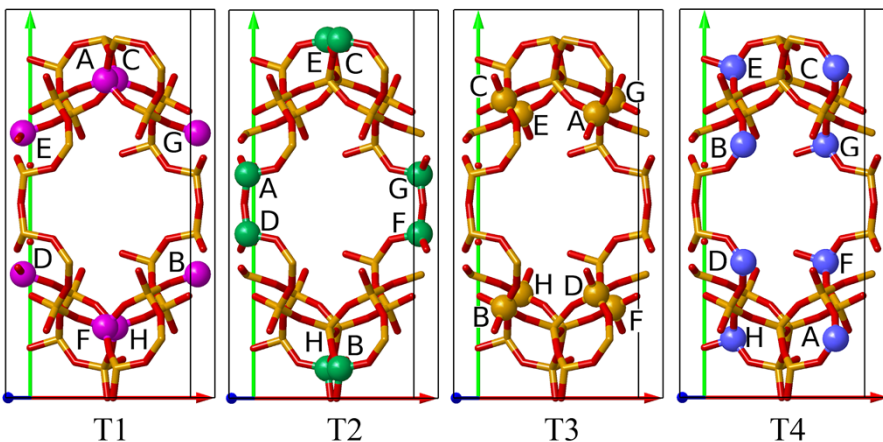


Figure S8. Color representation of the labeled T crystallographic sites of the RTH framework according to IZA. The 8 sites of every T group have been labelled with letters. T1, T2, T3 and T4 sites are depicted in pink, green, orange and blue respectively.

According to the IZA database⁵ the calcined pure silica RTH has four inequivalent T sites, namely T1, T2, T3 and T4, each with multiplicity 8. Because the calcined RTH unit cell contains 32 Si atoms there are 496 possible ways of arranging the two fluoride anions (r) in the 32 Si sites (n).

$$m = \frac{n!}{(n-r)!r!} m = \frac{n!}{(n-r)!r!} m = \frac{n!}{(n-r)!r!}$$

$$m = \frac{\frac{n!}{n!}}{(n-r)!r!} m = \frac{\frac{n!}{n!}}{(n-r)!r!} m = \frac{\frac{n!}{n!}}{(n-r)!r!}$$

$$1 m = \frac{n!}{(n-r)!r!}$$

However, two F^- bonded to two different T sites will have different chemical environments and consequently different chemical shifts, which would not agree with the ^{19}F NMR results. We have considered only combinations of two F^- in equivalent crystallographic sites. That yields a total of 112 combinations, 28 for each of the four sites (equation 1 with $n = 8$ and $r = 2$). For every combination exchanging the two F^- produces the same chemical structure, that is why we have calculated m combinations of r objects from a set of n objects (equation 1) because the order does not matter. In summary, for each crystallographic site (T1, T2, T3, T4), the 8 Si atoms have been labelled A, B, C, D, E, F, G, H and pairs of F^- have been located in 28 combinations without repetition, namely, AB, AC, AD, AE, ... GH. **Figure S8** shows the labels for every T crystallographic site. Each set with 28 structures is called a T group.

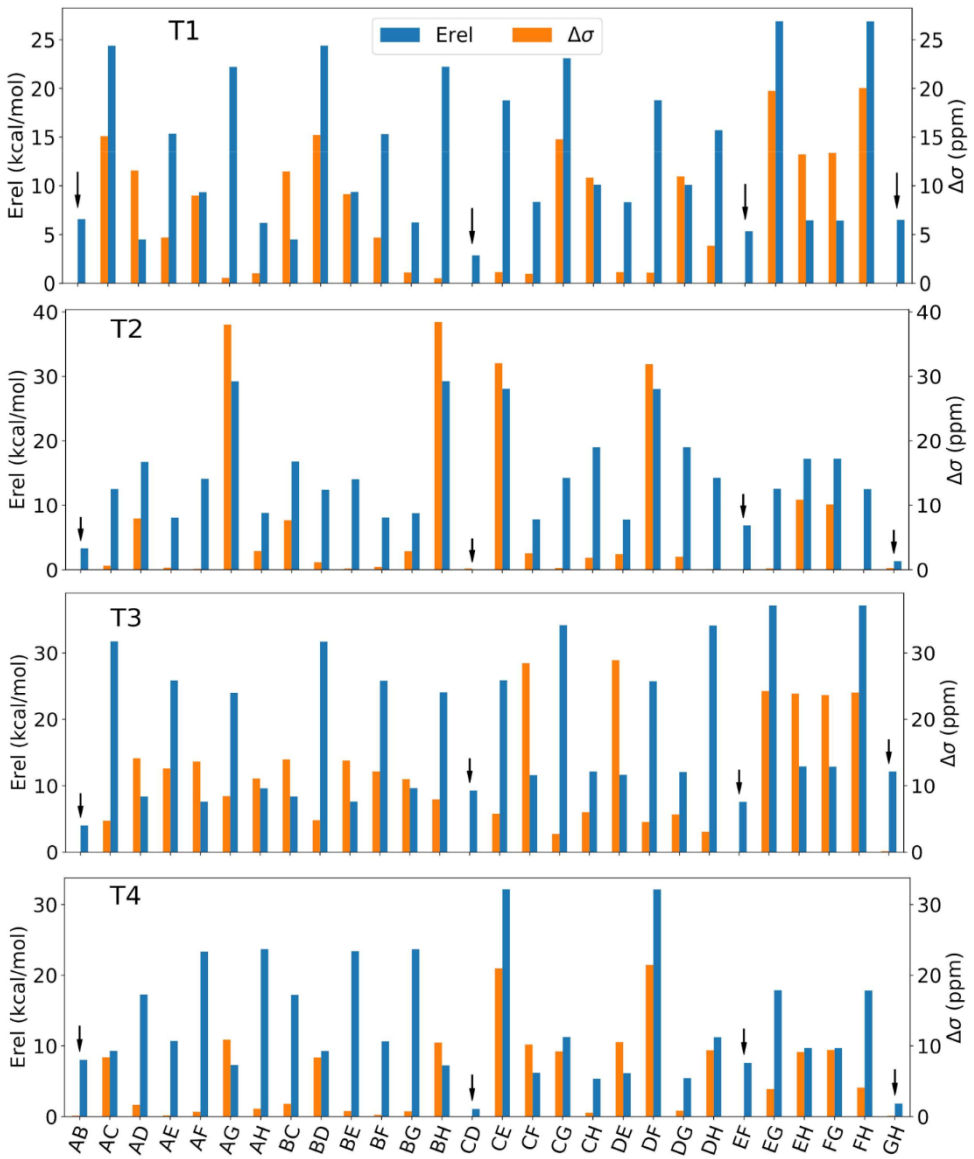


Figure S9. Relative energy (blue) in kcal/mol with respect to the most stable structure (CD of T2) and absolute difference ($\Delta\sigma_{\text{iso}}$) between the calculated shieldings of the two F^- of every structure. Arrows mark the 16 structures with equivalent F^- anions ($\Delta\sigma_{\text{iso}} \approx 0$).

Figure S9 shows the relative energy of the 112 models with respect to the most stable (CD model of the T2 group) and the difference of the absolute shielding between both fluorides ($\Delta\sigma_{\text{iso}}$) for each model. In general, when $\Delta\sigma_{\text{iso}} >> 1$ the corresponding structure is relatively unstable. The opposite is not necessarily true. Some models with $\Delta\sigma_{\text{iso}} \approx 0$ are also relatively unstable (e.g AF of T2 and T4). The $\Delta\sigma_{\text{iso}}$ is zero for the models AB, CD, EF, GH (marked with an arrow) of the four T groups, meaning that both F^- are chemically equivalent, according to the observed results by ^{19}F NMR. Moreover, in these 16 models the 32 Si atoms can be grouped in 16 equivalent pairs (see Tables S2, S3, S4, S5), that is, there are 16 different calculated ^{29}Si σ_{iso} which agrees with the 16 signals observed in the ^{29}Si NMR results. These is not true for the rest of the 96 models.

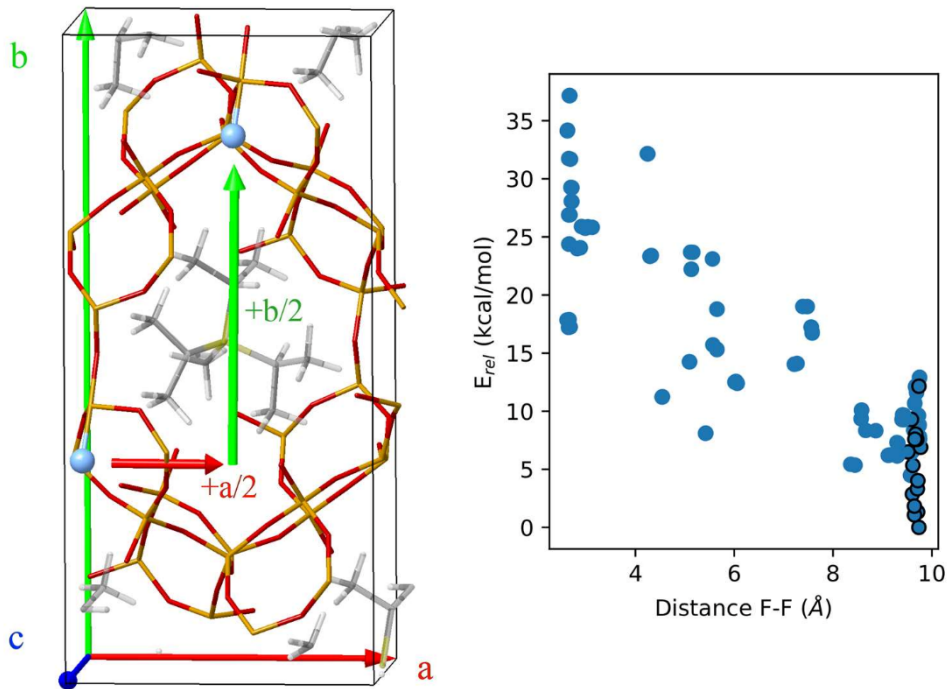


Figure S10. Representation of two equivalent fluoride anions (left panel). Si, O, P, C, H, F are depicted in orange, red, yellow, gray, light gray, blue respectively. Unit cell vectors a , b and c are depicted in red, green and blue respectively. The right panel shows the relative energy as a function of the shortest F-F distance. Circles corresponding to models with equivalent pairs of fluorides have a black border.

A close inspection of these 16 models (Tables S2 to S5) reveals that the two equivalent F^- are related by the following symmetry operation: $x+\frac{1}{2}$, $y+\frac{1}{2}$, z (left). The same holds for the 16 Si pairs. These 16 particular configurations are among the most stable because the distance between both fluoride anions is maximized (right). Analysis of the symmetry shows that there is no space group with the symmetry operations $(x, y, z; x+\frac{1}{2}, y+\frac{1}{2}, z)$ found in the best 16 models and consequently the unit cell must be redefined.

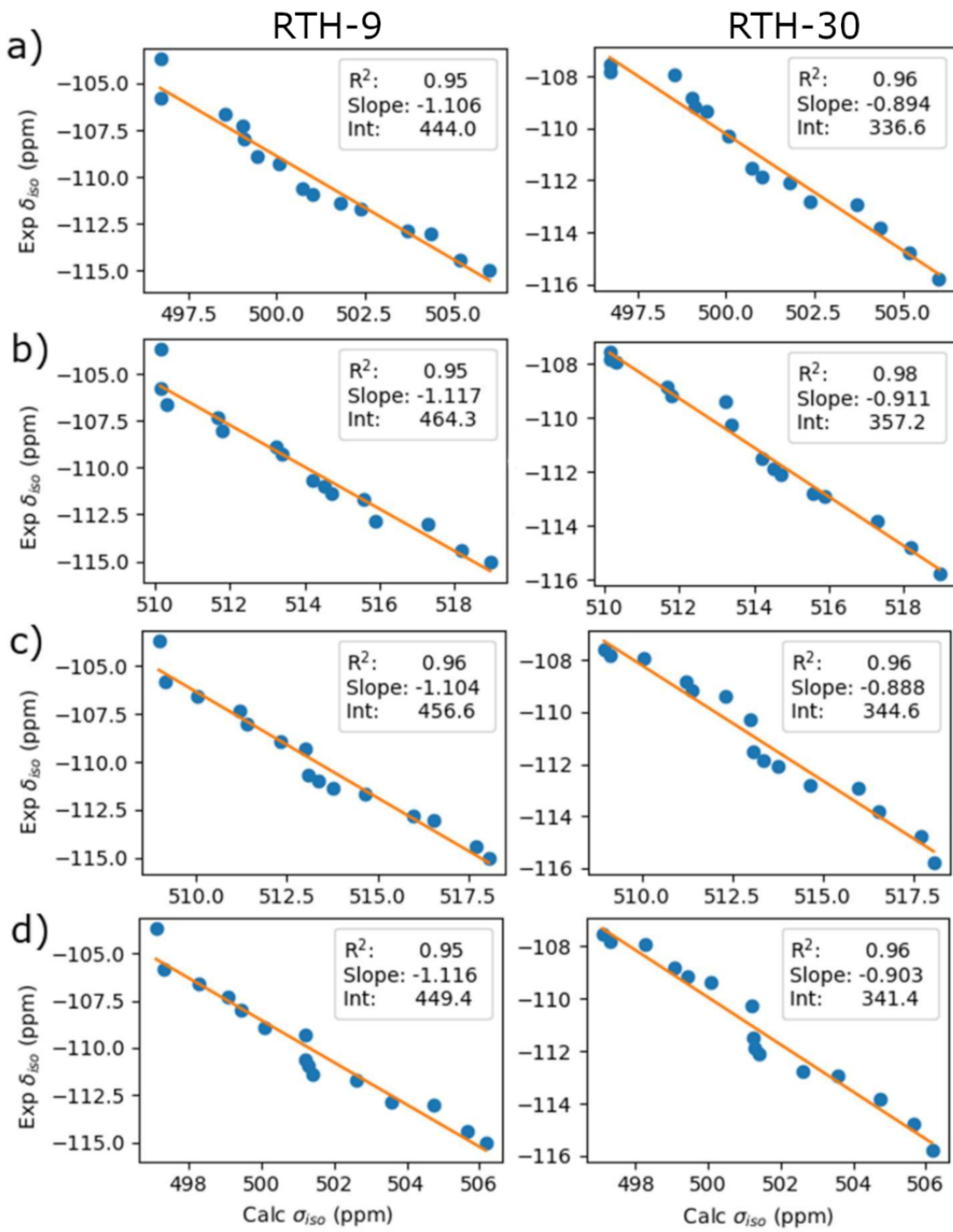


Figure S11. Correlation of the calculated $\sigma_{iso}^{29}\text{Si}$ of the models 5 (a), 6 (b), 7 (c) and 8 (d) with the experimental $\delta_{iso}^{29}\text{Si}$ of samples RTH-9 and RTH-30. In the four models, the fluoride anion is located in the T2 sites. Notice how the distinctive ^{29}Si signal at -103.70 ppm is not predicted properly with these models.

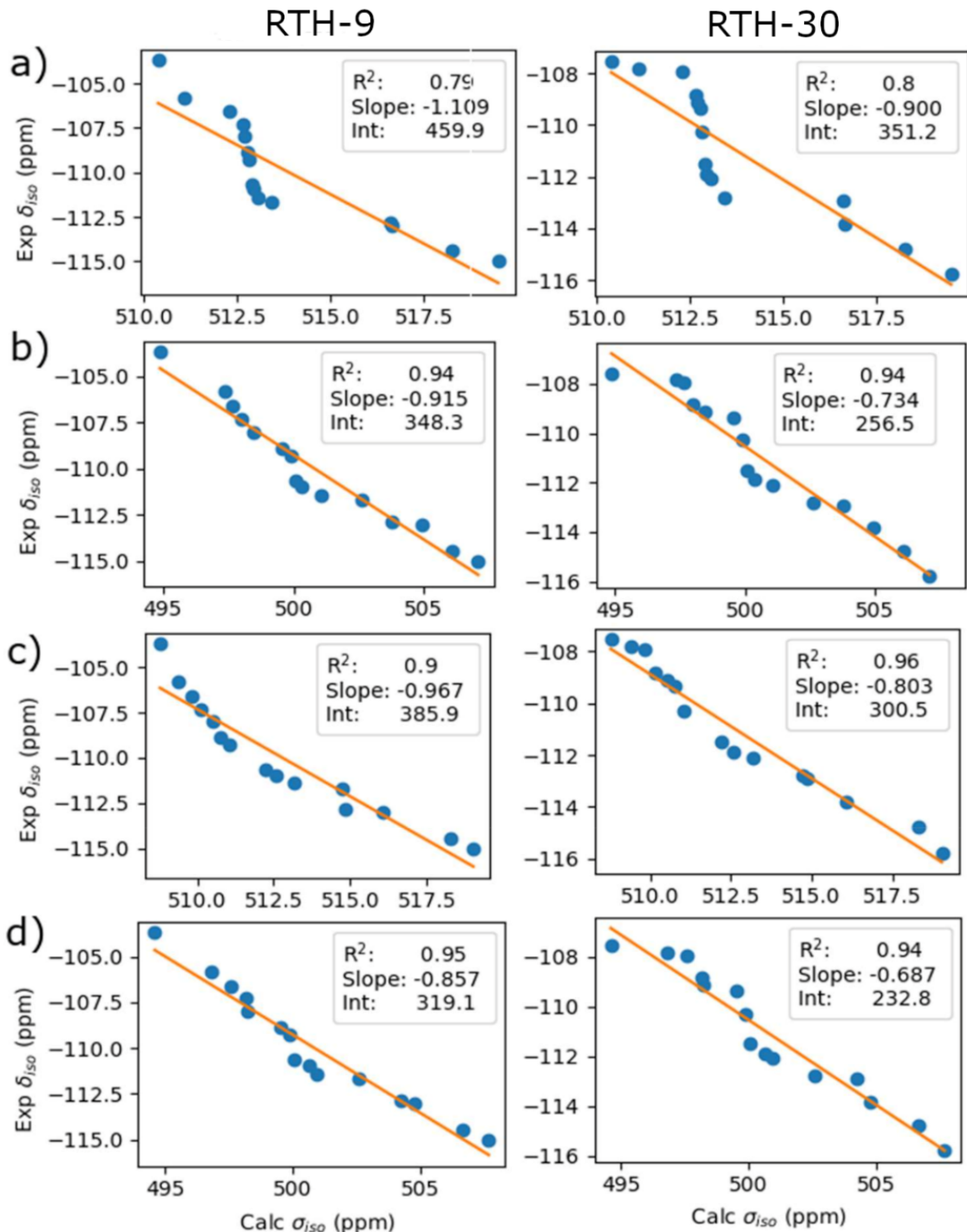


Figure S12. Correlation of the calculated $\sigma_{\text{iso}}^{29}\text{Si}$ of the models 9-II (a), 10-I (b), 11-II (c) and 12-II (d) with the experimental $\delta_{\text{iso}}^{29}\text{Si}$ of samples RTH-9 and RTH-30. In the four models, the fluoride anion is located in T3 sites.

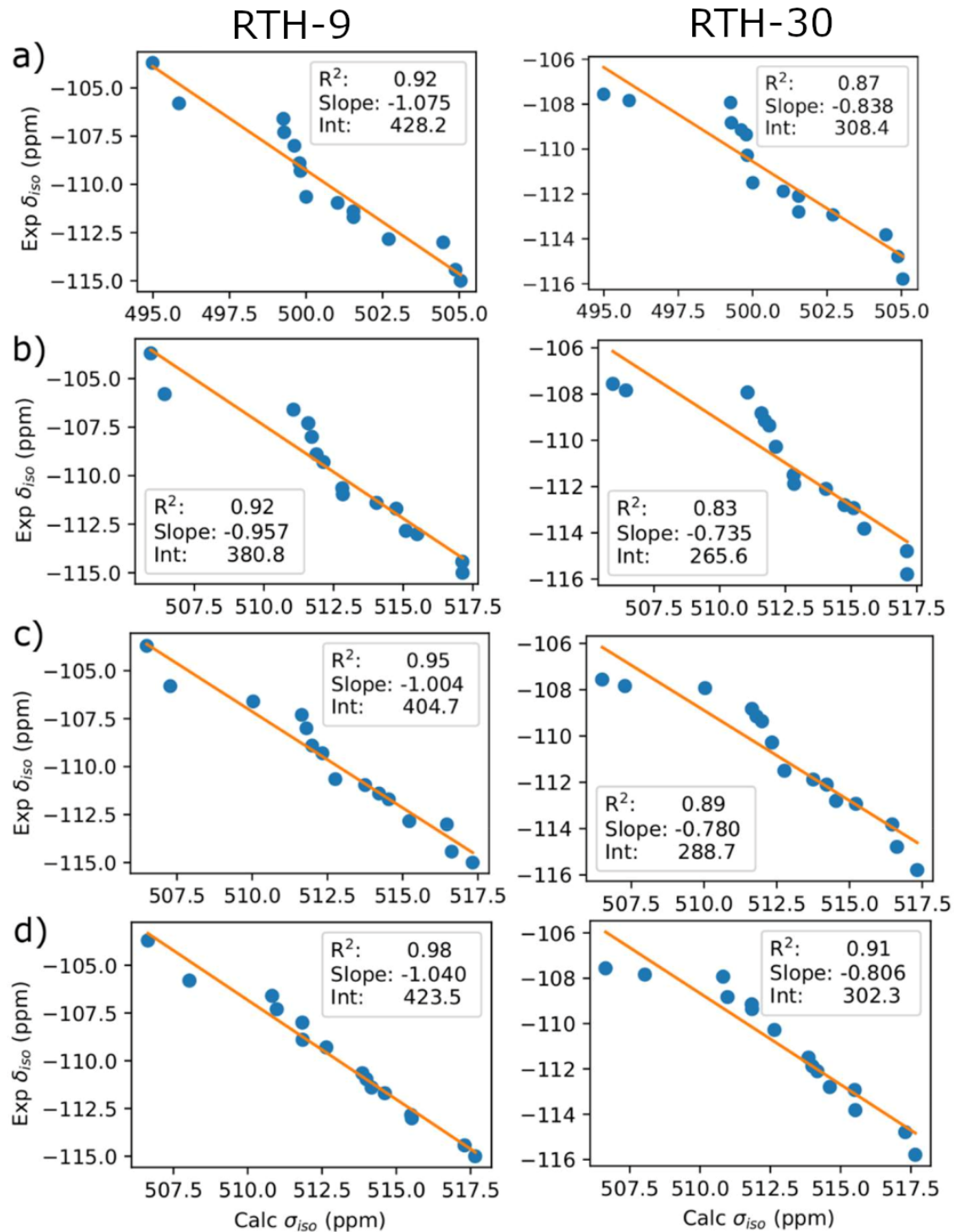


Figure S13. Correlation of the calculated $\sigma_{iso}^{29}\text{Si}$ of the models 13-I (a), 14-II (b), 15-II (c) and 16-I (d) with the experimental $\delta_{iso}^{29}\text{Si}$ of samples RTH-9 and RTH-30. In the four models, the fluoride anion is located in T4 sites. Notice how the distinctive ^{29}Si signal at -103.70 ppm well predicted with these models. Their correlation is better with the signals of sample RTH-9.

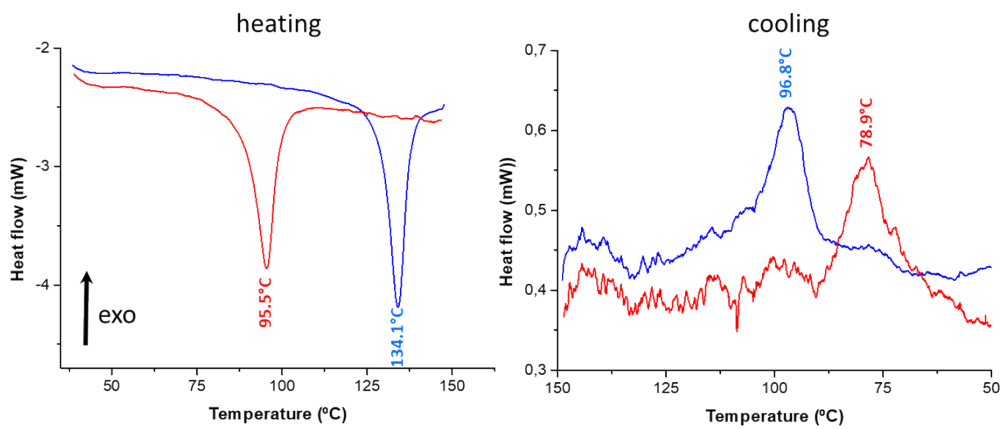


Figure S14. Plot of the heat flow against the temperature of the RTH-9 (red lines) and RTH-30 (blue line) samples upon heating from 25 °C to 150 °C (left graphical) and subsequent cooling down to 25 °C.

Table S1. Experimental $\delta_{iso}^{19}\text{F}$ (ppm) and theoretical $\sigma_{iso}^{19}\text{F}$ (ppm) values calculated with the modified Becke-Johnson exchange potential (TB-mBJ).⁶ The linear regression curve is shown in **Figure S2**.

| Fluorinated compound | σ_{iso} (TB-mBJ) | Experimental δ_{iso} |
|---|-------------------------|-----------------------------|
| LiF | 426.7 | -204.3 ¹ |
| NaF | 449.8 | -224.2 ¹ |
| KF | 358.4 | -133.3 ¹ |
| RbF | 328.9 | -90.9 ¹ |
| RbF.H ₂ O | 334.1 | -113.0 ¹ |
| MgF ₂ | 422.0 | -197.3 ¹ |
| SrF ₂ | 317.3 | -108.0 ¹ |
| AlF ₃ | 397.8 | -172.0 ¹ |
| CdF ₂ | 416.9 | -192.1 ² |
| HgF ₂ | 411.3 | -196.4 ² |
| KF.2H ₂ O | 350.9 | -133.0 ² |
| Na ₃ AlF ₆ | 417.8 | -189.0 ² |
| | 417.6 | -190.0 ² |
| Na ₅ Al ₃ F ₁₄ | 394.2 | -166.0 ² |
| | 416.4 | -182.0 |
| | 417.6 | -190.0 |
| Na ₂ SiF ₆ | 378.3 | -151.0 ² |
| α -PbF ₂ | 290.7 | -57.7 ² |
| | 263.1 | -20.5 |
| CF ₃ Cl | 259.2 | -28.6 ³ |
| CFCl ₂ CFCl ₂ | 298 | -67.8 ³ |
| SiF ₄ | 383.1 | -163.3 ³ |

Table S2. Starting coordinates for the OSDA in RTH-9 calculated from the PXRD data assuming a monoclinic unit cell.

| Site | Atom | x | y | z | Occ |
|------|------|------------|------------|-----------|---------|
| Si1 | Si | -0.0051 | 0.32152 | 0.34147 | 1.00000 |
| Si2 | Si | 0.40750 | 0.07430 | 0.12146 | 1.00000 |
| Si3 | Si | 0.25162 | 0.26300 | 0.22563 | 1.00000 |
| Si4 | Si | 0.15757 | 0.15369 | 0.01243 | 1.00000 |
| O1 | O | 0.14666 | 0.29105 | 0.32484 | 1.00000 |
| O2 | O | 0.00000 | 0.34596 | 0.50000 | 1.00000 |
| O3 | O | 0.95855 | 0.38251 | 0.24957 | 1.00000 |
| O4 | O | 0.88215 | 0.26671 | 0.31713 | 1.00000 |
| O5 | O | 0.24697 | 0.09169 | 0.06434 | 1.00000 |
| O6 | O | 0.40001 | 0.00000 | 0.17549 | 1.00000 |
| O7 | O | 0.50000 | 0.08342 | 0.00000 | 1.00000 |
| O8 | O | 0.30689 | 0.32309 | 0.13588 | 1.00000 |
| O9 | O | 0.18024 | 0.21066 | 0.12395 | 1.00000 |
| O10 | O | 0.00000 | 0.12915 | 0.00000 | 1.00000 |
| P1 | P | 0.4924(6) | 0.4975(2) | 0.5683(7) | 0.25000 |
| C1 | C | 0.5270(11) | 0.4105(3) | 0.5609(9) | 0.25000 |
| C2 | C | 0.3599(7) | 0.5194(5) | 0.4312(9) | 0.25000 |
| C3 | C | 0.6516(7) | 0.5421(4) | 0.5476(9) | 0.25000 |
| C4 | C | 0.4357(14) | 0.5173(7) | 0.7347(8) | 0.25000 |
| C5 | C | 0.415(3) | 0.3701(7) | 0.622(3) | 0.25000 |
| C6 | C | 0.547(4) | 0.3875(7) | 0.415(2) | 0.25000 |
| C7 | C | 0.2122(8) | 0.5121(16) | 0.471(3) | 0.25000 |
| C8 | C | 0.3834(15) | 0.5857(13) | 0.367(4) | 0.25000 |
| C9 | C | 0.747(2) | 0.5463(12) | 0.684(2) | 0.25000 |
| C10 | C | 0.621(2) | 0.6104(9) | 0.487(3) | 0.25000 |

Space Group: C 2/m; $a = 9.7395(14)$ Å, $b = 20.663(4)$ Å, $c = 9.8167(16)$ Å, alpha = 90°, beta = 96.130(12)°, gamma = 90°, Volume = 1964.3(5) Å³

Table S3. Starting coordinates for the OSDA in RTH-30 calculated from the PXRD data assuming a monoclinic unit cell

| Site | Atom | x | y | z | Occ |
|------|------|-------------|-------------|-------------|---------|
| Si1 | Si | 0.00620(6) | 0.32066(3) | 0.34168(5) | 1.00000 |
| Si2 | Si | 0.41203(6) | 0.07415(2) | 0.12222(6) | 1.00000 |
| Si3 | Si | 0.26103(6) | 0.26464(3) | 0.22335(7) | 1.00000 |
| Si4 | Si | 0.15786(5) | 0.15543(3) | 0.02331(7) | 1.00000 |
| O1 | O | 0.16206(6) | 0.29567(4) | 0.33051(8) | 1.00000 |
| O2 | O | 0.00000 | 0.34190(6) | 0.50000 | 1.00000 |
| O3 | O | 0.97178(10) | 0.38359(3) | 0.25312(8) | 1.00000 |
| O4 | O | 0.89808(7) | 0.26446(4) | 0.30391(10) | 1.00000 |
| O5 | O | 0.25235(6) | 0.09430(3) | 0.07868(10) | 1.00000 |
| O6 | O | 0.42281(14) | 0.00000 | 0.15671(14) | 1.00000 |
| O7 | O | 0.50000 | 0.09324(6) | 0.00000 | 1.00000 |
| O8 | O | 0.29855(10) | 0.32158(4) | 0.12218(7) | 1.00000 |
| O9 | O | 0.17395(9) | 0.21075(4) | 0.13581(8) | 1.00000 |
| O10 | O | 0.00000 | 0.13067(6) | 0.00000 | 1.00000 |
| P1 | P | 0.48615(5) | 0.49905(2) | 0.55516(7) | 0.25000 |
| C1 | C | 0.51170(10) | 0.41228(3) | 0.55706(10) | 0.25000 |
| C2 | C | 0.35922(8) | 0.52091(3) | 0.40991(9) | 0.25000 |
| C3 | C | 0.64952(7) | 0.53902(4) | 0.53555(10) | 0.25000 |
| C4 | C | 0.42461(14) | 0.52430(7) | 0.71809(9) | 0.25000 |
| C5 | C | 0.3810(3) | 0.37503(7) | 0.5838(4) | 0.25000 |
| C6 | C | 0.5705(3) | 0.38757(7) | 0.4257(3) | 0.25000 |
| C7 | C | 0.2433(2) | 0.47083(5) | 0.3829(4) | 0.25000 |
| C8 | C | 0.2999(2) | 0.58872(4) | 0.4254(4) | 0.25000 |
| C9 | C | 0.7582(2) | 0.52820(11) | 0.6613(3) | 0.25000 |
| C10 | C | 0.63129(19) | 0.61101(7) | 0.5023(4) | 0.25000 |

Space Group: $C\ 2/m$; $a = 9.7663(4)$ Å, $b = 20.8514(10)$ Å, $c = 9.6875(4)$ Å, $\alpha = 90^\circ$, $\beta = 96.342(3)^\circ$, $\gamma = 90^\circ$, Volume = $1960.71(15)$ Å³

Table S4. Calculated absolute shielding ($\sigma_{\text{iso}}^{29}\text{Si}$, ppm) of the 16 Si atoms (multiplicity of two) of the optimized monoclinic RTH model (32 Si atoms) with combinations of two F⁻ anions in **T1** sites.

| No | AB | | CD | | EF | | GH | |
|----|-----------|--------|-----------|--------|-----------|--------|-----------|--------|
| 1 | 436.61 | 436.6 | 436.88 | 436.85 | 436.51 | 436.5 | 435.74 | 435.73 |
| 2 | 438.78 | 438.75 | 437.6 | 437.59 | 437.96 | 437.95 | 436.46 | 436.45 |
| 3 | 439.77 | 439.77 | 439.18 | 439.15 | 440.07 | 440.06 | 438.04 | 438.04 |
| 4 | 440.84 | 440.81 | 439.9 | 439.88 | 440.31 | 440.28 | 438.42 | 438.41 |
| 5 | 440.99 | 440.93 | 440.27 | 440.23 | 440.41 | 440.41 | 439.78 | 439.78 |
| 6 | 441.12 | 441.11 | 440.38 | 440.36 | 440.43 | 440.43 | 440.33 | 440.32 |
| 7 | 441.65 | 441.58 | 440.94 | 440.89 | 440.87 | 440.84 | 441.22 | 441.22 |
| 8 | 442.28 | 442.26 | 440.97 | 440.95 | 441.25 | 441.24 | 441.65 | 441.65 |
| 9 | 442.39 | 442.36 | 441.06 | 441.05 | 441.27 | 441.25 | 441.92 | 441.92 |
| 10 | 442.49 | 442.48 | 442.23 | 442.23 | 442.15 | 442.11 | 442.39 | 442.39 |
| 11 | 442.55 | 442.5 | 442.35 | 442.29 | 443.07 | 443.06 | 443.3 | 443.3 |
| 12 | 442.89 | 442.87 | 442.51 | 442.49 | 443.12 | 443.09 | 443.57 | 443.57 |
| 13 | 444.75 | 444.72 | 443.84 | 443.77 | 443.29 | 443.25 | 443.74 | 443.71 |
| 14 | 448.31 | 448.28 | 447.11 | 447.04 | 447.35 | 447.33 | 447.02 | 447.01 |
| 15 | 449.29 | 449.25 | 447.59 | 447.51 | 447.67 | 447.65 | 447.12 | 447.11 |
| 16 | 462.85 | 462.84 | 462.54 | 462.52 | 461.5 | 461.48 | 459.88 | 459.86 |

Table S5. Calculated absolute shielding ($\sigma_{\text{iso}}^{29}\text{Si}$, ppm) of the 16 Si atoms (multiplicity of two) of the optimized monoclinic RTH model (32 Si atoms) with combinations of two F^- anions in **T2** sites.

| | AB | | CD | | EF | | GH | |
|----|-----------|--------|-----------|--------|-----------|--------|-----------|--------|
| 1 | 432.91 | 432.91 | 434.47 | 434.45 | 434.13 | 434.09 | 434 | 433.98 |
| 2 | 434.91 | 434.90 | 435.37 | 435.37 | 435.12 | 435.12 | 434.98 | 434.91 |
| 3 | 437.01 | 436.98 | 437.41 | 437.38 | 436.84 | 436.83 | 437.49 | 437.46 |
| 4 | 437.54 | 437.48 | 437.45 | 437.42 | 437.24 | 437.23 | 438.66 | 438.66 |
| 5 | 438.71 | 438.65 | 439.33 | 439.27 | 439.31 | 439.3 | 438.87 | 438.83 |
| 6 | 438.77 | 438.76 | 439.59 | 439.52 | 441.87 | 441.87 | 439.00 | 438.9 |
| 7 | 440.09 | 440.05 | 439.93 | 439.83 | 442.29 | 442.29 | 439.37 | 439.28 |
| 8 | 441.03 | 441.03 | 440.57 | 440.4 | 442.44 | 442.41 | 440.18 | 440.13 |
| 9 | 441.50 | 441.49 | 441.5 | 441.43 | 442.76 | 442.74 | 440.21 | 440.19 |
| 10 | 442.50 | 442.36 | 441.52 | 441.51 | 443.1 | 443.08 | 440.78 | 440.77 |
| 11 | 443.87 | 443.86 | 443.8 | 443.76 | 443.42 | 443.4 | 444.12 | 444.09 |
| 12 | 444.01 | 444.00 | 444.35 | 444.29 | 443.73 | 443.72 | 444.53 | 444.47 |
| 13 | 444.93 | 444.86 | 444.95 | 444.94 | 444.13 | 444.12 | 445.22 | 445.19 |
| 14 | 445.87 | 445.83 | 446.17 | 446.17 | 445.71 | 445.71 | 445.24 | 445.24 |
| 15 | 446.02 | 446.02 | 446.79 | 446.77 | 445.94 | 445.93 | 446.69 | 446.68 |
| 16 | 466.17 | 466.17 | 465.74 | 465.7 | 466.92 | 466.92 | 465.57 | 465.54 |

Table S6. Calculated absolute shielding ($\sigma_{\text{iso}}^{29}\text{Si}$, ppm) of the 16 Si atoms (multiplicity of two) of the optimized monoclinic RTH model (32 Si atoms) with combinations of two F^- anions in **T3** sites.

| | AB | | CD | | EF | | GH | |
|----|-----------|--------|-----------|--------|-----------|--------|-----------|--------|
| 1 | 432.19 | 432.19 | 434.06 | 434.03 | 429.95 | 429.94 | 434.57 | 434.53 |
| 2 | 433.66 | 433.66 | 434.27 | 434.18 | 434.57 | 434.57 | 436.7 | 436.58 |
| 3 | 437.04 | 436.97 | 434.59 | 434.54 | 437.79 | 437.76 | 436.92 | 436.82 |
| 4 | 437.91 | 437.86 | 436.96 | 436.94 | 438.35 | 438.31 | 437.15 | 437.11 |
| 5 | 437.96 | 437.93 | 438.46 | 438.41 | 438.52 | 438.44 | 438.15 | 438.08 |
| 6 | 438.12 | 438.08 | 438.94 | 438.9 | 439.11 | 439.05 | 439.16 | 439.05 |
| 7 | 438.22 | 438.2 | 439.15 | 439.08 | 439.97 | 439.96 | 440.46 | 440.43 |
| 8 | 438.31 | 438.31 | 439.23 | 439.16 | 440.18 | 440.16 | 440.83 | 440.8 |
| 9 | 439.16 | 439.13 | 439.49 | 439.36 | 441.57 | 441.55 | 440.93 | 440.91 |
| 10 | 439.77 | 439.77 | 440.35 | 440.34 | 441.67 | 441.61 | 441.85 | 441.82 |
| 11 | 442.83 | 442.79 | 442.8 | 442.77 | 441.69 | 441.68 | 442.22 | 442.18 |
| 12 | 443.57 | 443.54 | 443.92 | 443.89 | 442.3 | 442.27 | 444.24 | 444.09 |
| 13 | 445.43 | 445.4 | 446.13 | 446.07 | 444.55 | 444.54 | 445.27 | 445.24 |
| 14 | 446.74 | 446.73 | 446.42 | 446.41 | 446.67 | 446.65 | 445.54 | 445.49 |
| 15 | 448.49 | 448.49 | 447.74 | 447.73 | 448.26 | 448.19 | 447.64 | 447.61 |
| 16 | 464.93 | 464.91 | 469.23 | 469.14 | 466.22 | 466.2 | 469.27 | 469.22 |

Table S7. Calculated absolute shielding ($\sigma_{\text{iso}}^{29}\text{Si}$, ppm) of the 16 Si atoms (multiplicity of two) of the optimized monoclinic RTH model (32 Si atoms) with combinations of two of two F⁻ anions in **T4** sites.

| | AB | | CD | | EF | | GH | |
|----|-----------|--------|-----------|--------|-----------|--------|-----------|--------|
| 1 | 430.94 | 430.9 | 433.25 | 433.16 | 432.79 | 432.6 | 433.33 | 433.19 |
| 2 | 434.38 | 434.35 | 434.48 | 434.42 | 435.43 | 435.42 | 435.15 | 435.1 |
| 3 | 436.97 | 436.97 | 436.36 | 436.31 | 436.30 | 436.06 | 436.88 | 436.83 |
| 4 | 438.56 | 438.49 | 437.37 | 437.35 | 437.23 | 437.07 | 438.22 | 438.21 |
| 5 | 438.87 | 438.81 | 439.34 | 439.28 | 437.83 | 437.74 | 438.38 | 438.35 |
| 6 | 439.28 | 439.26 | 439.73 | 439.71 | 439.04 | 438.93 | 439.66 | 439.63 |
| 7 | 439.75 | 439.73 | 440.19 | 440.1 | 439.64 | 439.51 | 439.86 | 439.78 |
| 8 | 440.21 | 440.19 | 440.27 | 440.24 | 440.06 | 439.97 | 440.07 | 439.95 |
| 9 | 440.39 | 440.35 | 440.81 | 440.7 | 440.32 | 440.28 | 440.8 | 440.79 |
| 10 | 441.29 | 441.28 | 440.93 | 440.83 | 440.45 | 440.39 | 440.89 | 440.81 |
| 11 | 441.65 | 441.63 | 441.89 | 441.88 | 442.33 | 442.22 | 441.94 | 441.87 |
| 12 | 443.69 | 443.67 | 442.78 | 442.77 | 443.75 | 443.71 | 442.16 | 442.1 |
| 13 | 444.99 | 444.96 | 443.89 | 443.82 | 443.88 | 443.82 | 443.41 | 443.37 |
| 14 | 445.23 | 445.19 | 444.28 | 444.19 | 444.6 | 444.39 | 444.44 | 444.36 |
| 15 | 445.64 | 445.6 | 445.8 | 445.78 | 446.66 | 446.55 | 445.35 | 445.23 |
| 16 | 469.41 | 469.4 | 464.29 | 464.27 | 468.79 | 468.54 | 464.19 | 464.13 |

Table S8. Calculated absolute isotropic ^{29}Si shielding (σ_{iso} , ppm) of the RTH optimized models with a triclinic unit cell and the fluoride anion located in T1 and T2 sites. The σ_{iso} values of the model with the F⁻ anion in position 6 (in italics) were used to make the plot shown in Figure 8.

| T1 | T2 |
|-----------|-----------|
|-----------|-----------|

| 1 | 2 | 3 | 4 | 5 | 6 | 7 | 8 |
|----------|----------|----------|----------|----------|---------------|----------|----------|
| 498.83 | 498.77 | 509.15 | 497.79 | 496.72 | <i>510.14</i> | 508.96 | 497.11 |
| 499.77 | 499.95 | 509.7 | 499.29 | 496.74 | <i>510.16</i> | 509.12 | 497.31 |
| 499.8 | 500.18 | 509.8 | 499.56 | 498.54 | <i>510.30</i> | 510.04 | 498.26 |
| 499.86 | 500.27 | 511.17 | 499.58 | 499.03 | <i>511.67</i> | 511.21 | 499.09 |
| 500.41 | 500.44 | 512.6 | 499.7 | 499.1 | <i>511.77</i> | 511.38 | 499.45 |
| 500.89 | 500.49 | 512.9 | 500.87 | 499.46 | <i>513.25</i> | 512.33 | 500.09 |
| 501.34 | 501.05 | 513.8 | 501.65 | 500.07 | <i>513.40</i> | 512.99 | 501.22 |
| 502.03 | 501.23 | 513.86 | 501.69 | 500.73 | <i>514.21</i> | 513.08 | 501.23 |
| 502.5 | 502.58 | 514.01 | 502.03 | 501.00 | <i>514.51</i> | 513.37 | 501.29 |
| 503 | 502.67 | 514.1 | 503.18 | 501.78 | <i>514.72</i> | 513.78 | 501.43 |
| 503.36 | 502.82 | 515.12 | 503.18 | 502.37 | <i>515.59</i> | 514.67 | 502.63 |
| 503.9 | 502.84 | 516.12 | 503.74 | 503.68 | <i>515.90</i> | 515.97 | 503.59 |
| 504.99 | 503.47 | 516.93 | 504.68 | 504.37 | <i>517.29</i> | 516.57 | 504.75 |
| 506.44 | 506.37 | 518.45 | 506.6 | 505.17 | <i>518.19</i> | 517.72 | 505.68 |
| 507.14 | 506.81 | 519.00 | 506.95 | 506.02 | <i>518.96</i> | 518.07 | 506.17 |
| 524.52 | 527.46 | 537.67 | 523.9 | 530.37 | <i>545.27</i> | 544.25 | 530.59 |

Table S9. Calculated absolute isotropic ^{29}Si shielding (σ_{iso} , ppm) of the RTH optimized models with a triclinic unit cell and the fluoride anion located in T3 sites.

| 9-I | 9-II | 10-I | 10-II | 11-I | 11-II | 12-I | 12-II |
|------------|-------------|-------------|--------------|-------------|--------------|-------------|--------------|
| 494.06 | 510.38 | 494.88 | 509.58 | 495.78 | 508.79 | 494.61 | 507.21 |
| 497.68 | 511.09 | 497.35 | 509.67 | 496.76 | 509.4 | 496.79 | 510.54 |
| 498.42 | 512.29 | 497.67 | 510.27 | 498.48 | 509.83 | 497.58 | 510.75 |
| 498.71 | 512.63 | 498.01 | 510.34 | 498.79 | 510.14 | 498.15 | 510.83 |
| 499.16 | 512.68 | 498.45 | 511.17 | 500.35 | 510.54 | 498.25 | 511.33 |
| 499.39 | 512.77 | 499.58 | 512.33 | 500.57 | 510.74 | 499.51 | 511.35 |
| 499.85 | 512.79 | 499.9 | 512.83 | 500.57 | 511.04 | 499.85 | 512.32 |
| 500.46 | 512.9 | 500.08 | 512.99 | 500.65 | 512.22 | 500.06 | 512.34 |
| 500.79 | 512.92 | 500.33 | 513.42 | 501.18 | 512.56 | 500.61 | 512.50 |
| 501.30 | 513.05 | 501.08 | 513.52 | 501.2 | 513.16 | 500.91 | 513.05 |
| 502.23 | 513.4 | 502.58 | 514.41 | 502.15 | 514.73 | 502.57 | 513.59 |
| 502.64 | 516.58 | 503.76 | 515.1 | 503.24 | 514.84 | 504.24 | 513.82 |
| 504.61 | 516.63 | 504.89 | 515.87 | 503.47 | 516.06 | 504.75 | 516.69 |
| 506.05 | 518.26 | 506.06 | 520.31 | 507.32 | 518.29 | 506.64 | 517.92 |
| 508.00 | 519.48 | 507.07 | 520.58 | 508.16 | 519.01 | 507.65 | 520.08 |
| 530.31 | 547.98 | 535.29 | 545.14 | 530.41 | 549.2 | 534.79 | 544.63 |

Table S10. Calculated absolute isotropic ^{29}Si shieldings (σ_{iso} , ppm) of the RTH optimized models with a triclinic unit cell and the fluoride anion located in T4 sites. The σ_{iso} values of the model with the F atom in position 16-I (in italics) were used to make the plot shown in Figure 9.

| 13-I | 13-II | 14-I | 14-II | 15-I | 15-II | 16-I | 16-II |
|-------------|--------------|-------------|--------------|-------------|--------------|---------------|--------------|
| 494.99 | 507.24 | 496.49 | 508.07 | 509.27 | 506.50 | <i>506.64</i> | 495.86 |
| 495.85 | 508.15 | 497.38 | 509.03 | 510.67 | 507.28 | <i>508.04</i> | 497.25 |
| 499.26 | 509.67 | 497.83 | 512.26 | 512.61 | 510.03 | <i>510.82</i> | 498.00 |
| 499.28 | 510.68 | 498.93 | 512.97 | 512.86 | 511.65 | <i>510.98</i> | 498.73 |
| 499.62 | 511.55 | 499.27 | 513.27 | 513.31 | 511.80 | <i>511.84</i> | 499.07 |
| 499.79 | 511.71 | 499.87 | 513.4 | 513.73 | 511.99 | <i>511.85</i> | 499.88 |
| 499.82 | 512.11 | 500.30 | 513.42 | 514.46 | 512.34 | <i>512.65</i> | 499.99 |
| 500.00 | 512.92 | 500.79 | 513.57 | 515.21 | 512.76 | <i>513.86</i> | 500.98 |
| 501.03 | 513.81 | 500.86 | 513.84 | 515.91 | 513.75 | <i>514.00</i> | 501.24 |
| 501.55 | 513.85 | 501.14 | 514.1 | 515.91 | 514.22 | <i>514.17</i> | 501.6 |
| 501.55 | 515.79 | 501.15 | 514.44 | 516.19 | 514.54 | <i>514.62</i> | 501.74 |
| 502.7 | 516.24 | 503.68 | 514.57 | 516.32 | 515.22 | <i>515.50</i> | 503.19 |
| 504.48 | 516.40 | 504.27 | 516.31 | 517.17 | 516.47 | <i>515.52</i> | 503.6 |
| 504.88 | 517.12 | 504.38 | 518.08 | 518.57 | 516.63 | <i>517.30</i> | 504.49 |
| 505.05 | 517.59 | 505.85 | 520.06 | 518.84 | 517.33 | <i>517.65</i> | 505.48 |
| 532.53 | 543.50 | 528.58 | 544.45 | 542.21 | 546.92 | <i>546.33</i> | 528.52 |

Table S11. Cell parameters and volume of the triclinic unit cell of models 6 and 16-I and those obtained experimentally from the XRD data for the RTH-A, RTH-B and RTH-C phases.

| RTH Phase | <i>a</i> (Å) | <i>b</i> (Å) | <i>c</i> (Å) | α (°) | β (°) | γ (°) | Volume(Å ³) |
|------------|--------------|--------------|--------------|--------------|-------------|--------------|-------------------------|
| Model 6 | 9.7422 | 11.5000 | 9.7902 | 86.464 | 96.324 | 116.049 | 979.3 |
| Model 16-I | 9.794 | 11.396 | 9.7111 | 87.879 | 96.642 | 115.970 | 967.8 |
| RTH-A | 9.7265(5) | 11.3864(6) | 9.8017(5) | 87.853(3) | 96.205(3) | 114.988(3) | 978.12(8) |
| RTH-B | 9.7516(4) | 11.5072(3) | 9.6825(2) | 87.327(2) | 96.330(2) | 115.102(2) | 977.90(5) |
| RTH-C | 9.7376(3) | 11.4669(3) | 9.7640(2) | 87.446(2)° | 96.068(2)° | 115.069(2)° | 982.01(5) |

References

1. Martinez-Ortigosa, J.; Simancas, J.; Vidal-Moya, J. A.; Gaveau, P.; Rey, F.; Alonso, B.; Blasco, T., Host–Guest and Guest–Guest Interactions of P- and N-Containing Structure Directing Agents Entrapped inside MFI-Type Zeolite by Multinuclear NMR Spectroscopy. *The Journal of Physical Chemistry C* **2019**, *123* (36), 22324-22334.
2. Fyfe, C. A.; Brouwer, D. H.; Lewis, A. R.; Villaescusa, L. A.; Morris, R. E., Combined Solid State NMR and X-ray Diffraction Investigation of the Local Structure of the Five-Coordinate Silicon in Fluoride-Containing As-Synthesized STF Zeolite. *Journal of the American Chemical Society* **2002**, *124* (26), 7770-7778.
3. Fyfe, C. A.; Brouwer, D. H.; Lewis, A. R.; Chézeau, J.-M., Location of the Fluoride Ion in Tetrapropylammonium Fluoride Silicalite-1 Determined by $^{1}\text{H}/^{19}\text{F}/^{29}\text{Si}$ Triple Resonance CP, REDOR, and TEDOR NMR Experiments. *Journal of the American Chemical Society* **2001**, *123* (28), 6882-6891.
4. Koller, H.; Wölker, A.; Villaescusa, L. A.; Díaz-Cabañas, M. J.; Valencia, S.; Camblor, M. A., Five-Coordinate Silicon in High-Silica Zeolites. *Journal of the American Chemical Society* **1999**, *121* (14), 3368-3376.
5. Ch. Baerlocher and L.B. McCusker, Database of Zeolite Structures. <http://www.iza-structure.org/databases/>.
6. Tran, F.; Blaha P., Accurate Band Gaps of Semiconductors and Insulators with a Semilocal Exchange-Correlation Potential. *Physical Review Letters* **2009**, *102*, (22), 22641.